Electronic Supplementary Material (ESI) for Nanoscale.

Electronic Supplementary Information

Layer-separated MoS_2 bearing reduced graphene oxide formed by an *in-situ* intercalation-cum-anchoring route mediated by $Co(OH)_2$ as a Pt-free electrocatalyst for oxygen reduction

Rajith Illathvalappil [a], Sreekuttan M. Unni [a,b], and Sreekumar Kurungot [a,b] *.

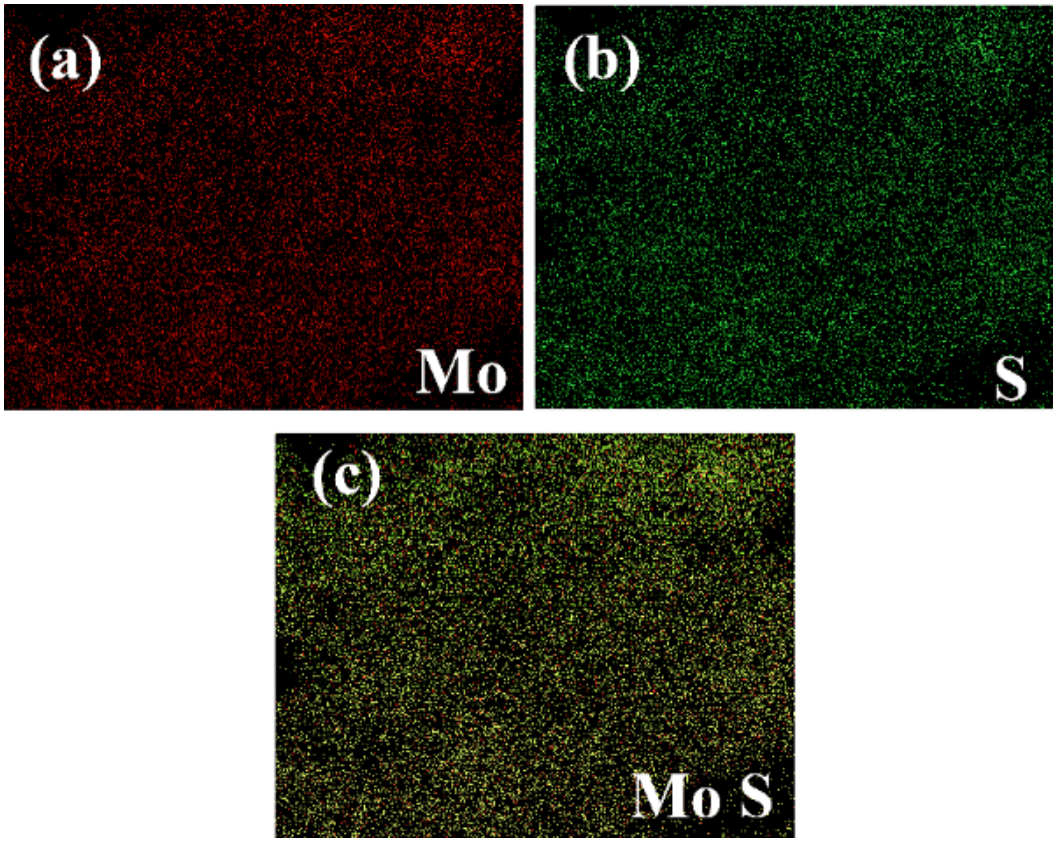

Fig. S1. SEM elemental mapping of MoS_2-P (a) molybdenum, (b) sulphur and (c) molybdenum and sulphur combined.

The SEM elemental mapping of molybdenum (Figure S1a) and sulphur (Figure S1b) clearly reveals the presence of Mo and S in MoS_2-P, which shows a nearly homogeneous distribution.

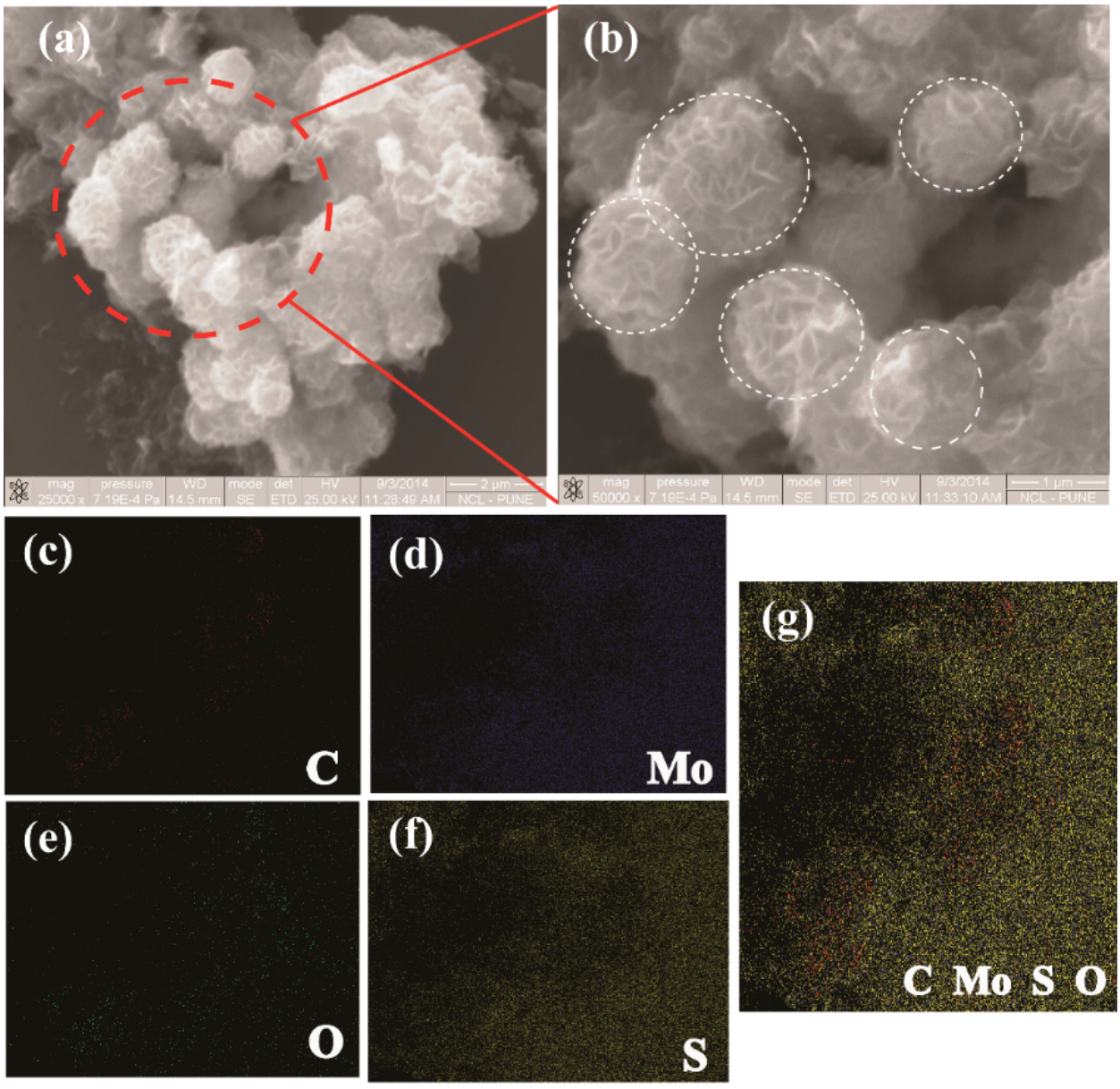

Fig. S2. SEM images of MoS_2/rGO and the corresponding elemental mapping.

SEM images of MoS_2/rGO (Figure S2a and S2b) show a flower like shape with more exposed edge surface compared to the as synthesized MoS_2 (*i.e.* MoS_2-P). The white dotted circles (Figure S2b) indicate the flower like growth pattern of MoS_2/rGO. The Mo (Figure S2d) and S (Figure S2f) mappings depict that the MoS_2 phase is well dispersed on the rGO surface. Apart from the C, Mo and S moieties,

MoS_2/rGO also shows presence of oxygen (Figure S2e), which could be arising from the functional groups from rGO and also from the oxides of molybdenum.

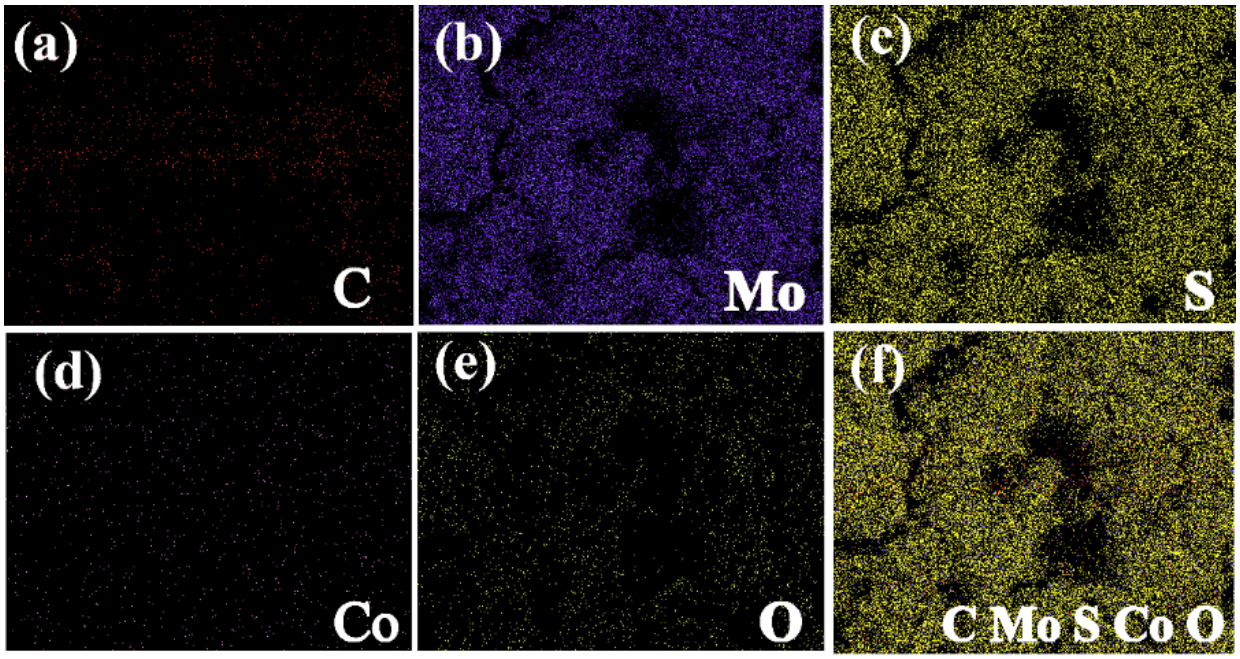

Fig. S3. SEM elemental mapping of $Co(OH)_2$-MoS_2/rGO.

As the intensity of the carbon is found to be lower compared to the molybdenum and sulphur in the SEM elemental mapping, it can be concluded that both molybdenum and sulphur are covered very well above the carbon support. Cobalt (Figure S3d) and oxygen (Figure S3e) mappings indicate that $Co(OH)_2$ is decorated on the surface of MoS_2, and the lower intensity of the cobalt indicates that the amount of cobalt is relatively less in the sample.

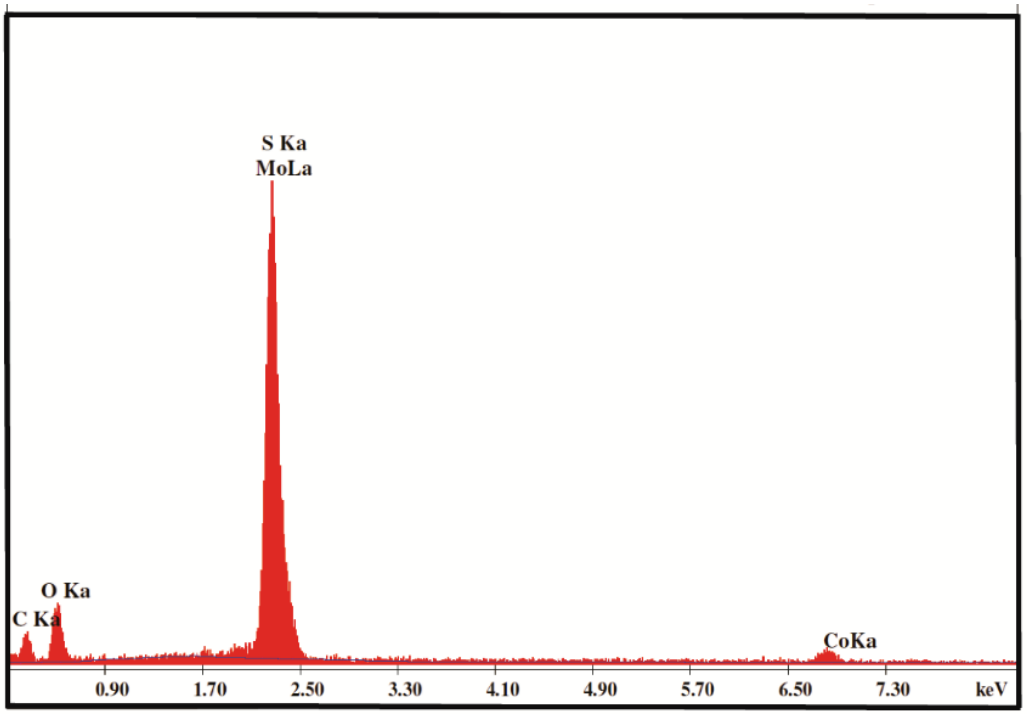

Fig. S4. EDAX spectrum of $Co(OH)_2$-MoS_2/rGO.

EDAX is providing the confirmation on cobalt in the sample. The amount of cobalt is comparatively less than that of Mo and S. Also, the peak for carbon also is found to be less in this case, which is attributed to the coverage of MoS_2 sheets on rGO.

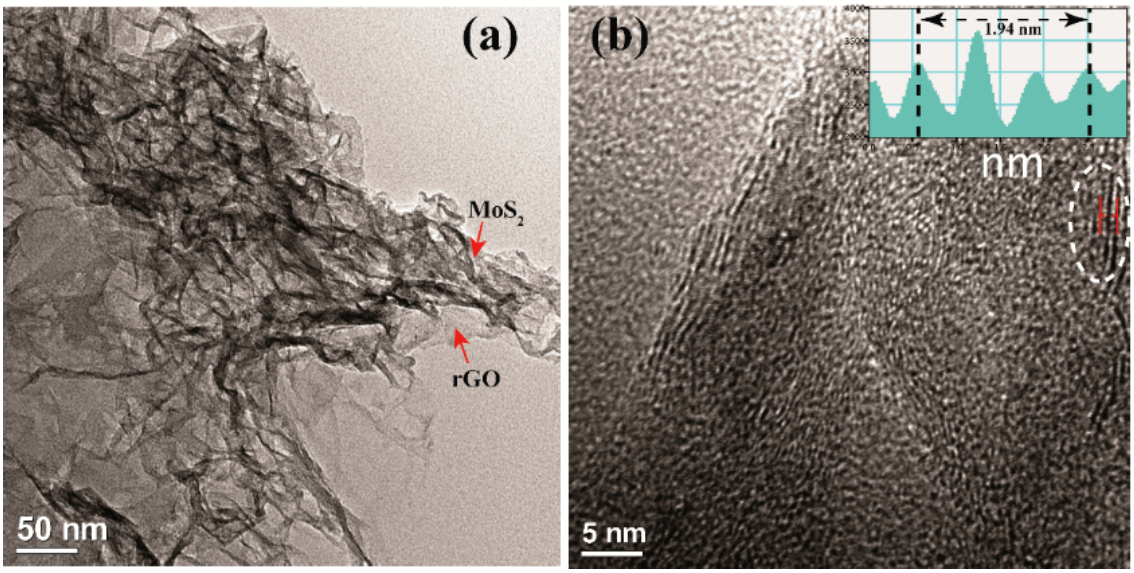

Fig. S5. TEM image of a) MoS_2/rGO and b) magnified image of MoS_2/rGO

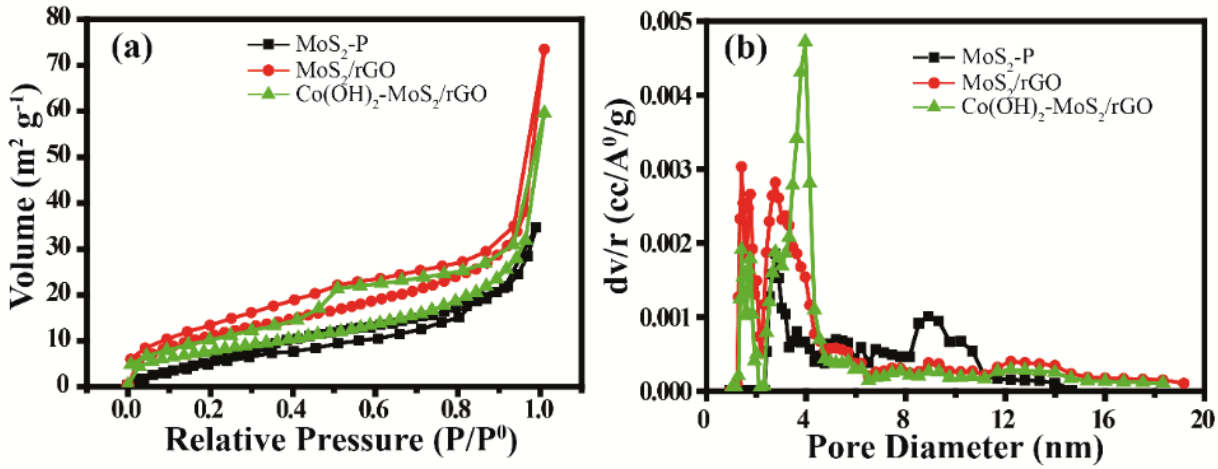

Fig. S6. (a) N_2 adsorption-desorption isotherm profiles of MoS_2-P, MoS_2/rGO and $Co(OH)_2$-MoS_2/rGO and (b) pore size distribution profiles of MoS_2-P, MoS_2/rGO and $Co(OH)_2$-MoS_2/rGO.

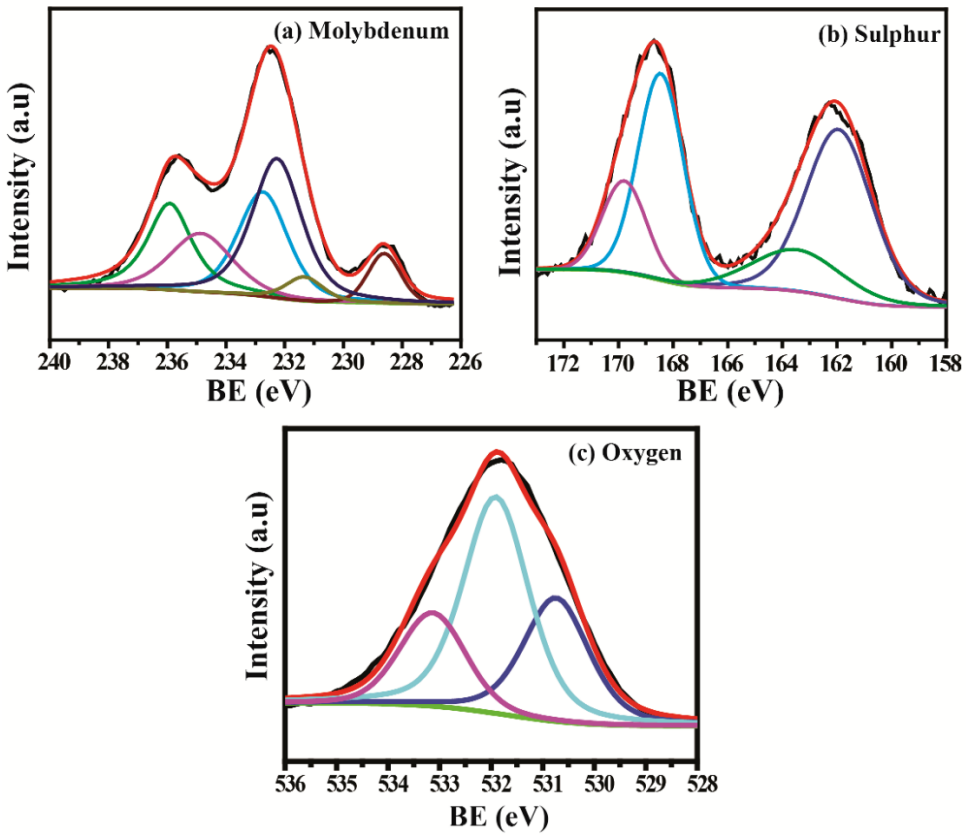

Fig. S7. Deconvoluted XPS of MoS_2-P (a) molybdenum, (b) sulphur and (c) oxygen. The black line corresponds to the raw data and the red line represents the fitted data.

The XPS of MoS_2-P depicts the peak for molybdenum, sulphur and oxygen. The deconvoluted XPS of molybdenum (Figure S7a) shows the peaks at 228.6 and 231.3 eV corresponding to the $3d_{3/2}$ and $3d_{1/2}$ peak for Mo (IV) cation. The peaks at 232.7 and 235.9 eV show higher oxidation state of molybdenum and this suggests the presence of oxides of molybdenum also in the sample. The deconvoluted sulphur spectra (Figure S7b) show peaks at 161.8 and 163.3 eV for the $2p_{3/2}$ and $2p_{1/2}$ for the sulphide.[1] This confirms the presence of MoS_2 in the sample. The peak at 530.7 eV corresponding to the O 1s peak for MoO_3.[2] The peak at 532 eV depicts the peak for physically adsorbed oxygen molecules.[3]

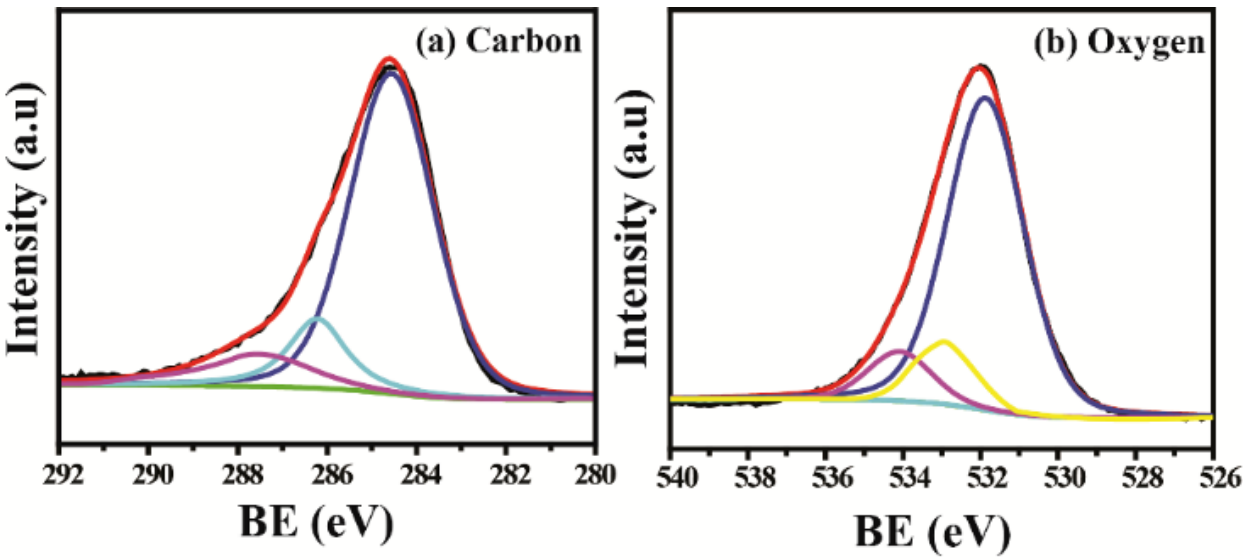

Fig. S8. Deconvoluted XPS of (a) carbon and (b) oxygen in $Co(OH)_2$-MoS_2/rGO. The black curve corresponds to the raw data and the red curve represents the fitted data.

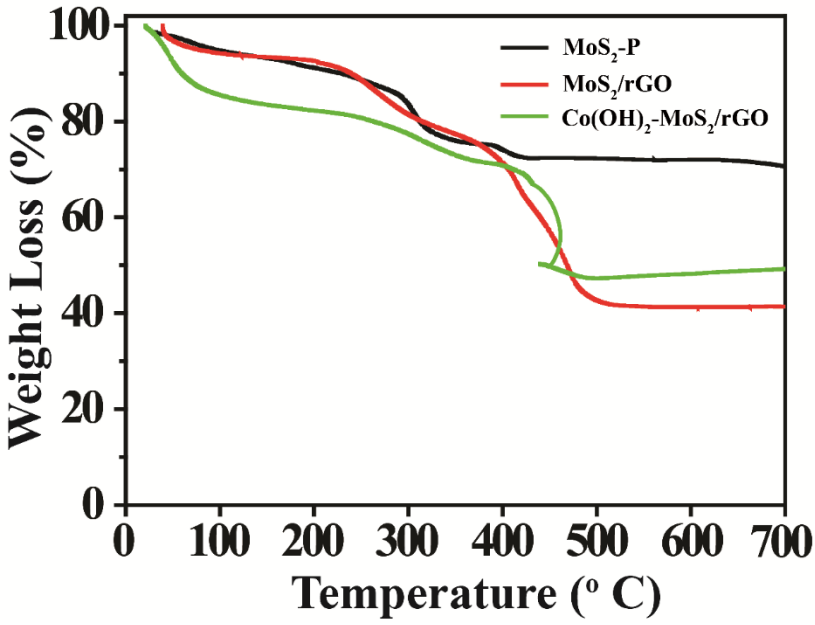

Figure S9: TGA analysis of MoS_2-P, MoS_2/rGO and $Co(OH)_2$-MoS_2/rGO.

Thermo gravimetric analysis (TGA) of MoS_2-P, MoS_2/rGO and $Co(OH)_2$-MoS_2/rGO was carried out in air atmosphere from room temperature to 700 °C with a heating rate of 10°/min to find out the weight percentage of $Co(OH)_2$, MoS_2 and rGO in the $Co(OH)_2MoS_2$/rGO composite. The initial weight loss from room temperature to 200 °C was mainly attributed to the removal of the physisorbed/chemisorbed water molecules. Above 300 °C, a sudden drop in the weight was observed for the MoS_2-P, MoS_2/rGO and $Co(OH)_2$-MoS_2/rGO samples. This is attributed to the transformation of MoS_2 into MoO_3. Above 400 °C, carbon would be converted into CO_2 and this can lead to a sudden weight loss for the MoS_2/rGO and $Co(OH)_2$-MoS_2/rGO samples. The $Co(OH)_2$ decomposition is expected to start in the range of 170-330 °C with the loss of OH group.[4] The weight percentages of rGO, MoS_2 and $Co(OH)_2$ in $Co(OH)_2$-MoS_2/rGO are approximately 50 wt%, 40 wt% and 10 wt% respectively.

Calibration of the reference electrode

To convert the potential from Hg/HgO to RHE, we have carried out LSV in hydrogen saturated 0.1 M KOH solution at a scan rate of 1 mV/s with Pt as the working electrode, Pt as the counter electrode

and Hg/HgO as the reference electrode. The potential at which the current crosses the zero line is taken as the correction factor.

So, E (RHE) = E (Hg/HgO) + 0.870

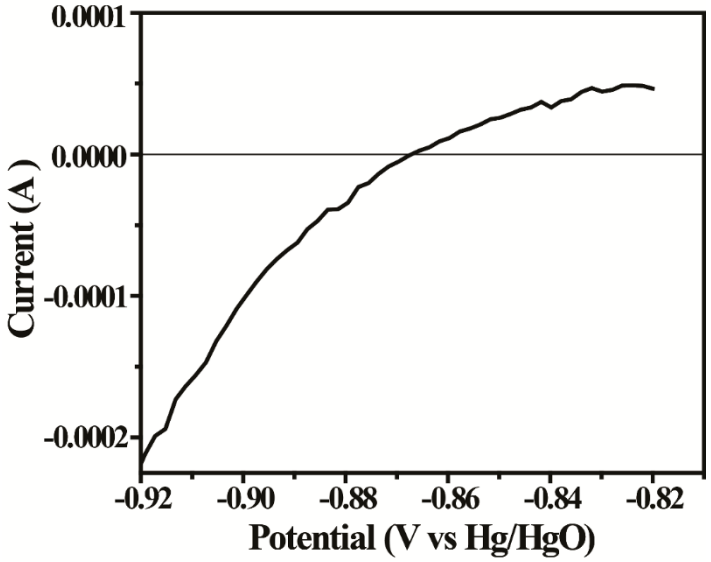

Fig. S10. Calibration curve for reference electrode.

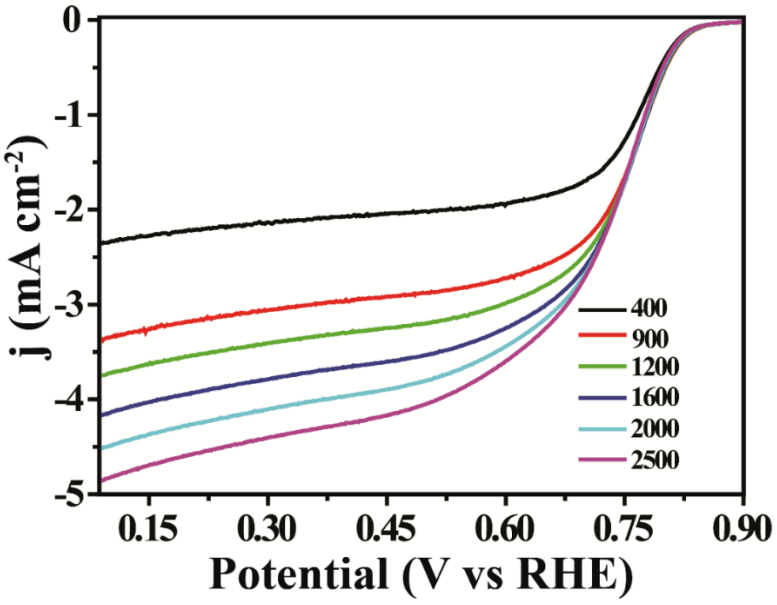

Fig. S11. Linear sweep voltammograms (LSVs) of $Co(OH)_2$-MoS_2/rGO with different rotation rates of the working electrode in 0.1 M KOH solution saturated with O_2. The potential scan rate was 5mV s^{-1} and Hg/HgO and a graphite rod were used as the reference and counter electrodes, respectively.

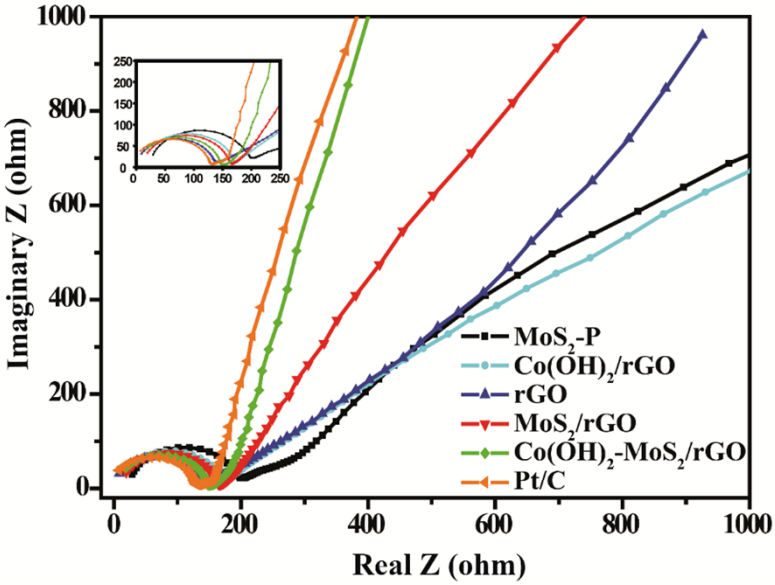

Figure S12: Nyquist plots of MoS_2-P, $Co(OH)_2$/rGO, rGO, MoS_2/rGO, $Co(OH)_2$-MoS_2/rGO and Pt/C. Inset shows the magnified portion of the plot at the high frequency range.

The electrochemical impedance (EIS) study was carried out in the frequency range of 10^6 Hz to 0.1 Hz with an AC amplitude of 10 mV in the open circuit voltage condition. The charge transfer resistance (R_{ct}) value of MoS_2-P is comparatively much higher (171.23 Ω) than that of the other samples (161.34, 153.61, 139.87 and 136.82 Ω respectively for $Co(OH)_2$/rGO, MoS_2/rGO, rGO and $Co(OH)_2$-MoS_2/rGO). This reveals the poor electrical conductivity for MoS_2-P as compared to the rest of the samples. The results clearly indicate that the presence of rGO in MoS_2 is helping the system to decrease its R_{ct} value (153.61 Ω). This, in other words, means that the incorporation of rGO in MoS_2 ultimately increases the electrical conductivity of the composite materials. Among the prepared samples, $Co(OH)_2$-MoS_2/rGO has the lowest R_{ct} value (136.82 Ω) and this infers that the electron movement is faster in this particular composite. This ultimately reflects to the improvement in the ORR performance of $Co(OH)_2$-MoS_2/rGO.

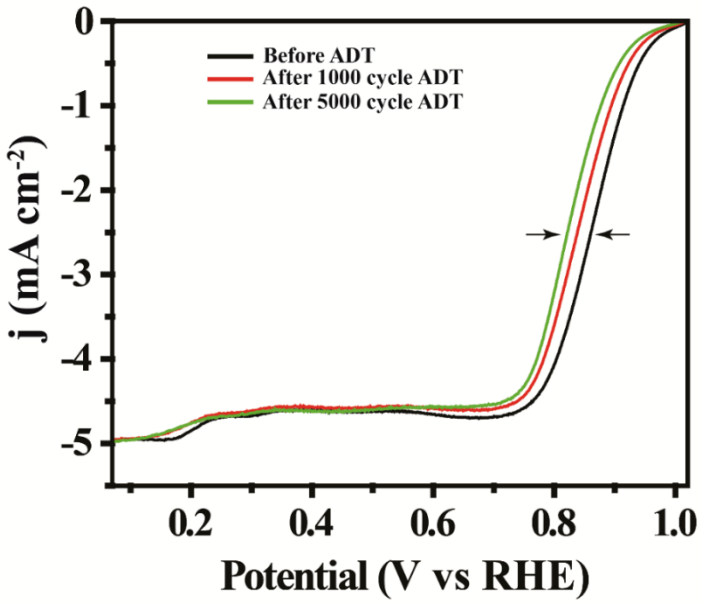

Fig. S13. LSVs for the durability test of 40 wt. % Pt/C in 0.1 M KOH solution saturated with O_2. The recording was done by maintaining a scan rate of 5mV s^{-1} and an electrode rotation speed of 1600 rpm.

Table S1. Electrical conductivity data of MoS_2-P, MoS_2/rGO and $Co(OH)_2$-MoS_2/rGO.

Sl.No.	Sample	Electrical Conductivity (S/cm)
1	MoS_2-P	0.0072
2	MoS_2/rGO	0.435
3	$Co(OH)_2$-MoS_2/rGO	0.609

Table S2. Comparison of the ORR performance of MoS_2-P, $Co(OH)_2$/rGO, rGO, MoS_2/rGO, $Co(OH)_2$-MoS_2/rGO and Pt/C.

Sl.No.	Catalyst	Onsetpotential (V)	$E_{1/2}$ (V)
1	MoS_2-P	0.708	0.349
2	$Co(OH)_2$/rGO	0.817	0.650
3	rGO	0.792	0.603
4	MoS_2/rGO	0.805	0.646
5	$Co(OH)_2$-MoS_2/rGO	0.855	0.731
6	Pt/C	0.963	0.860

Table S3. Comparison of the present study with few recent reports of MoS_2 for oxygen reduction reaction.

Sl. No.	Catalyst	Synthesis Method	Onset Potential (V)	Reference Electrode	Electrolyte	References
1	MoS_2	Exfoliation	-0.28	SCE	0.1 M KOH	5
2	AuNP/MoS_2 film	Drop casting	-0.10	SCE	0.1 M KOH	6
3	MoS_2 NDs/NGr	Hydrothermal	0.95	RHE	0.1 M KOH	7
4	MoS_2/NGr	Physical mixing	-0.12	SCE	0.1 M KOH	8
5	$Co(OH)_2$-MoS_2/rGO	Hydrothermal	0.855	RHE	0.1 M KOH	This work

References

1 C.-B. Ma, X. Qi, B. Chen, S. Bao, Z. Yin, X.-J. Wu, Z. Luo, J. Wei, H.-L. Zhang and H. Zhang, *Nanoscale*, 2014, **6**, 5624.

2 K. Dewangan, N. N. Sinha, P. K. Sharma, A. C. Pandey, N. Munichandraiah and N. S. Gajbhiye, *CrystEngComm*, 2011, **13**, 927.

3 H. Nan, Z. Wang, W. Wang, Z. Liang, Y. Lu, Q. Chen, D. He, P. Tan, F. Miao, X. Wang, J. Wang and Z. Ni, *ACS Nano*, 2014, **8**, 5738.

4 D. Ghosh, S. Giri and C. K. Das, *ACS Sustainable Chem. Eng.*, 2013, **1**, 1135.

5 T. Wang, D. Gao, J. Zhuo, Z. Zhu, P. Papakonstantinou, Y. Li and M. Li, *Chem. Eur. J.*, 2013, **19**, 11939.

6 T. Wang, J. Zhuo, Y. Chen, K. Du, P. Papakonstantinou, Z. Zhu, Y. Shao and M. Li, *ChemCatChem*, 2014, **6**, 1877.

7 C. Du, H. Huang, X. Feng, S. Wu and W. Song, *J. Mater. Chem. A*, 2015, **3**, 7616.

8 K. Zhao, W. Gu, L. Zhao, C. Zhang, W. Peng and Y. Xian, *Electrochim. Acta*, 2015, **169**, 142.